Dobslaw, H., Dill, R. (2018): Predicting Earth orientation changes from global forecasts of atmosphere-hydrosphere dynamics. - *Advances in Space Research*, *61*, 4, pp. 1047—1057.

DOI: http://doi.org/10.1016/j.asr.2017.11.044

Predicting Earth Orientation Changes from Global Forecasts of Atmosphere-Hydrosphere Dynamics

Henryk Dobslaw* and Robert Dill

Deutsches GeoForschungsZentrum – GFZ, Section 1.3: Earth System Modelling, Telegrafenberg, 14473 Potsdam, Germany.
dobslaw@gfz-potsdam.de, dill@gfz-potsdam.de

Abstract

Effective Angular Momentum (EAM) functions obtained from global numerical simulations of atmosphere, ocean, and land surface dynamics are routinely processed by the Earth System Modelling group at Deutsches GeoForschungsZentrum. EAM functions are available since January 1976 with up to 3 hours temporal resolution. Additionally, 6 days-long EAM forecasts are routinely published every day. Based on hindcast experiments with 305 individual predictions distributed over 15 months, we demonstrate that EAM forecasts improve the prediction accuracy of the Earth Orientation Parameters at all forecast horizons between 1 and 6 days. At day 6, prediction accuracy improves down to 1.76 mas for the terrestrial pole offset, and 2.6 mas for ΔUT1, which correspond to an accuracy increase of about 41% over predictions published in Bulletin A by the International Earth Rotation and Reference System Service.

Keywords: Earth rotation excitation; Earth orientation prediction; global geophysical fluids

1. Introduction

The orientation of the solid Earth with respect to inertial space is conventionally described by five Earth Orientation Parameters (EOP) comprising the celestial pole position (nutation), the terrestial pole coordinates (polar motion), and the non-uniform part of the angular spin velocity (ΔUT1). Daily EOP estimates are routinely provided by the International Earth Rotation and Reference Systems Service (IERS; *Bizouard and Gambis*, 2009), the most recent EOP 14 C04 series (abbreviated as C04 in the following) is

usually available with 30 days latency. Earth orientation parameters are determined from a realization of the International Terrestrial Reference System through instruments and observatories attached to the crust that provide various space geodetic observations. The latest realization, the International Terrestrial Reference Frame 2014 (ITRF2014; *Altamimi et al.*, 2016) is consistent with C04. The IERS also disseminates rapid EOP estimates and EOP predictions for up to 90 days into the future (Bulletin A), which are in particular important for real-time spacecraft navigation and the tracking of deep-space objects with terrestrial radio telescopes. A thorough evaluation of numerous alternative EOP prediction algorithms has been recently performed within the Earth Orientation Prediction Comparison Campaign (EOP-PCC; *Kalarus et al.*, 2010).

Dynamic causes for Earth orientation changes are conveniently studied by applying the principle of conservation of angular momentum in the system Earth including effects of external torques, internal mass-redistribution, and exchange of angular momentum of the solid Earth with atmosphere, oceans, and the terrestrial hydrosphere (*Gross*, 2007). Estimates of angular momentum changes due to mass transport in the geophysical fluid layers are available from atmospheric reanalyses (*Chen*, 2005), ocean state estimates (*Gross et al.*, 2003), and land data assimilation systems (*Nastula et al.*, 2007) as collected by the Global Geophysical Fluid Centre (GGFC) of the IERS. Even though mass transport on Earth has a small but non-negligible impact on nutation via tidal terms of nearly diurnal retrograde frequencies (see, e.g., *Schindelegger et al.*, 2016), it is in particular polar motion (PM) and ΔUT1 that are dominated by Earth system dynamics.

For some time already, atmospheric angular momentum estimates derived from operational numerical weather forecasts contribute to the prediction of ΔUT1 (*Freedman et al.*, 1994; *Gross et al.*, 1998; *Gambis et al.*, 2011), which is largely dominated by the effects of zonal tropospheric winds. For PM prediction, however, solely forecasted AAM do not yield noteable improvements since contributions from ocean dynamics and terrestrial water storage are also relevant (*Dill and Dobslaw*, 2010; *Dill et al.*, 2013). The Earth System Modelling group at Deutsches GeoForschungsZentrum (ESMGFZ) provides so-called Effective Angular Momentum (EAM $\chi_{1,2,3}$; *Brzeziński*, 1992) functions representing the effects of mass distribution and transport on the orientation of the Earth based on data from the European Centre for Medium-Range Weather Forecasts (ECMWF) and corresponding numerical simulations describing ocean and land surface dynamics (*Dobslaw et al.*, 2010). In addition, 6 days-long EAM forecasts for atmosphere, oceans, and the terrestrial hydrosphere are now routinely provided so that EAM-

based predictions of PM and ΔUT1 become possible by considering all three geophysical fluid layers consecutively.

In the following, we will outline the characteristics of the current set of EAM functions provided by ESMGFZ (Sect. 2), highlight the importance of atmospheric tides (Sect. 3) and discuss the quality of the routinely issued EAM forecasts for up to 6 days into the future (Sect. 4). Based on hindcast experiments (i.e., experimental forecasts starting at some time in the past so that those can be readily verified against already available final EOP estimates) extending over a period of 15 months, we finally demonstrate that the incorporation of forecasted EAM functions substantially improves predictions of ΔUT1 and PM over the current quality level of Bulletin A.

2. Effective Angular Momentum Functions from ESMGFZ

The atmospheric EAM functions (AAM) from ESMGFZ are based on analysis and forecast data out of global numerical weather prediction (NWP) models from the ECMWF. We use ERA-40 (*Uppala et al.*, 2005) for 1976–1978, ERA-Interim (*Dee et al.*, 2011) for 1979–2006, and operational NWP data from 2007 onwards. The different ECMWF data-sets are harmonized by mapping surface pressure to a common reference orography as outlined in *Dobslaw* (2016). A combination of 6-hourly analyses and 3-hourly forecasts is performed as suggested by *Dobslaw and Thomas* (2005). The inverse-barometric (IB) correction is applied over the ocean regions. AAM forecasts for up to 6 days into the future are calculated every day from the ECMWF high-resolution deterministic forecast initialized at 0 h UTC. The temporal resolution of those forecasts is 3 hours as well.

Ocean bottom pressure and baroclinic currents from an unconstrained simulation with the Max-Planck-Institute for Meteorology Ocean Model (MPIOM; *Jungclaus et al.*, 2013) are used for the calculation of ocean angular momentum functions (OAM). MPIOM is an ocean general circulation model discretized globally on an Arakawa-C grid in the horizontal and a z-grid in the vertical. We utilize a medium-resolution model configuration with a 1° tri-polar grid and 40 vertical layers. The model is forced with atmospheric surface pressure, wind stress, temperature, incoming solar radiation, and precipitation taken from the ECMWF data-sets introduced above. The additive-inverse IB correction is applied over the ocean regions for sake of consistency with the AAM. OAM forecasts for up to 6 days into the future are calculated once per day from a dedicated MPIOM model run that is forced with atmospheric conditions from the latest ECMWF high-resolution deterministic forecast.

Terrestrial water storage is simulated with the global Land Surface Discharge Model (LSDM; *Dill*, 2008). Physics are based on *Hagemann and Dümenil* (2003) and represent the dynamics of soil moisture, snow storage, as well as water stored in wetlands, rivers, and lakes. The model is discretized on a 0.5° equiangular grid and provides water storage and transport estimates at daily time intervals. Forecasts of hydrospheric angular momentum functions (HAM) for up to 6 days into the future are calculated once per day from a specific LSDM integration that is forced with atmospheric conditions obtained from the corresponding ECMWF forecast.

Further technical documentation and routinely updated plots of the most recent EAM time-steps are available from http://www.gfz-potsdam.de/en/esmdata. This web-site also provides access to the GRACE Atmosphere and Ocean De-Aliasing Level-1B Product (*Dobslaw et al.*, 2017) and to globally gridded elastic deformations of the Earth's crust caused by geophysical fluid loading (*Dill and Dobslaw*, 2013) that are based on identical mass distributions as the EAM functions discussed here. The final EAM series for atmosphere, oceans, and the terrestrial hydrosphere start in January 1976 and are routinely updated at about 10 h UTC with all 8 time-steps of the previous day. The associated 6 days-long EAM forecasts are typically available one hour later.

3. Separation of Tidal Signals

Daily estimates of polar motion and ΔUT1 as provided by C04 are considered to be free of diurnal and semi-diurnal tidal effects which were reduced during the processing of the space geodetic data, and we consequently attempt to exclude periodic signals at similar frequencies also from the model-based EAM functions. Tidal variations in the atmosphere are principally excited by two different mechanisms: First, absorption of solar radiation by both water vapor and ozone creates large periodic temperature variations in the middle atmosphere that propagate vertically as described by the thermal wind equations and cause large scale variations in atmospheric surface pressure. Secondly, tides in the atmosphere are excited by direct gravitational attraction of atmospheric masses from tide-generating bodies in the solar system, and more importantly also by periodic deformations of the lower boundary of the atmosphere related to both tides in the solid Earth and in the oceans.

We identify tidal variations at periods of 24, 12, and 8 h to be most important in atmospheric surface pressure and upper-air wind fields from

ECMWF. In addition, the major semi-diurnal lunar tide (12.41 h) is considered to be relevant as also recognized by, e.g., *Bizouard et al.* (2014). Since atmospheric tides are known to be slightly modulated over the year, two additional sidebands are estimated for each central frequency. Tides represented by ECMWF data-sets have been found to be susceptible to changes in both spatial resolution of the model and the evolution of the observing system (e.g., *Schindelegger and Dobslaw*, 2016). Tidal signals are therefore fitted and removed for each year individually during 1976 – 2006. For all later years, tides estimated over the period 2007 – 2014 are subtracted.

Exemplarily, we show amplitude spectra in the diurnal band estimated over the period 1976 – 2016 for the current AAM from ESMGFZ and its predecessor described in *Dobslaw et al.* (2010), which is labelled as GFZ2010 in the following (Fig. 1). We note dominant tidal signals at S_1 and its two sidebands K_1 and P_1 in the χ_1 component for both surface pressure and wind terms in GFZ2010, that are largely reduced in the current ESMGFZ data-set. For the axial component χ_3, sidebands in surface pressure are less prominent, but nevertheless estimated and removed as well for consistency. For the wind term, instead, even the consideration of more than two sidebands would be justified.

Since MPIOM is forced by ECMWF surface pressure and wind fields containing periodic variations associated with atmospheric tides, an oceanic response at identical frequencies is simulated by the numerical model. Tidal variations are therefore estimated and removed also from the bottom pressure and current fields prior to the calculation of OAM in a similar way as for the atmosphere. Here, we show amplitude spectra in the semi-diurnal band estimated over the period 1976 – 2016 (Fig. 2). We note that S_2 is the shortest period resolved from the 6-hourly sampling of GFZ2010, leading to an enhanced broadband variability at periods above 12 h due to temporal aliasing. Signals dominating GFZ2010 at the S_2, T_2, and to some extent also M_2 frequencies are entirely removed from ESMGFZ. We also note a distinct signal at K_2 persisting in ESMGFZ, since that period has not been included into the list of removed tidal lines.

4. EAM Forecast Verification

We perform a numerical hindcast experiment over the period June 2016 – August 2017 with in total 305 individual forecast runs for atmosphere, oceans, and terrestrial hydrosphere that are initialized at 0 h UTC and extend over a period of 6 days. We follow NWP standard procedures and

contrast any forecast with subsequently available analysis data of the particular time instance in order to assess the internal forecast quality by means of Brier skill scores (*von Storch and Zwiers*, 1999)

$$B_{\mathrm{F}}(t) = 1 - \frac{S^2_{\mathrm{F}}(t)}{S^2_{\mathrm{P}}(t)}. \tag{1}$$

Here, S^2_{F} represents the mean squared error (MSE) of the ESMGFZ forecast depending on leadtime t, and S^2_{P} the MSE of the persistent forecast taken from the final EAM value at the time of forecast initialization. As a rule of thumb, forecasts should have Brier scores of more than 0.6 to be effectively useful (*von Storch and Zwiers*, 1999).

Skill scores averaged over the full extent of the hindcast experiment reveal scores close to 1 for the HAM, since the terrestrial hydrosphere varies only slowly during 6 days and thus can be predicted with great confidence (Fig. 3). Skills are also high for surface pressure and bottom pressure terms with values well above 0.6 until day 6. For the equatorial wind terms χ_1 and χ_2 however, we note exceptionally poor scores for the first time-steps, that counter-intuitively improve during progression of the forecast and result in skill scores as high as 0.6 during day 4 and 5. Somewhat similar but less severe variations are also seen in the ocean current terms. Initial analysis suggests that quasi-periodic motions at periods close to 1.2 d corresponding to the atmospheric normal mode Ψ_1 are present in the forecasted wind fields that are not reproduced in a similar way in the final analysis.

As a preliminary solution to this problem, we smooth the forecasted equatorial wind terms with a 24h low-pass filter to reduce the daily variability before re-estimating skill scores (Fig. 4). Brier scores for χ_1 and χ_2 improve substantially and do not contain large variations between adjacent time-steps anymore. As a consequence, the skill scores for the sum of AAM, OAM and HAM improve as well. Scores gradually decay with forecast lead time but approach 0.6 only at day 6 for all three components, thereby indicating that EAM forecasts indeed contain effectively useful information over the whole forecast period considered here.

5. Prediction of Earth Rotation Parameters

We finally attempt utilizing EAM forecasts to predict polar motion and ΔUT1. A combination of least squares extrapolation and autoregressive modelling as recommended by *Kalarus et al.* (2010) is used to account for any remaining biases between the final EAM functions of ESMGFZ and

geodetic excitation functions as derived from C04. Signals with periods of 1, 1/2, and 1/3 years are estimated to account for any mis-modelled seasonal signals particularly related to the global mass balance (*Yan and Chao*, 2012) from a (moving) base-window of four years. An additional term with a period of 13.7 days is required to account for a prominent periodicity in C04 that is likely related to aliasing of sub-daily tide model errors (*Madzak et al.*, 2016).

For the set of 305 forecasts, nine individual prediction experiments are performed that differ from each other mostly in terms of the applied inital values. To arrive at quantitative accuracy estimates, predicted values are subtracted from C04, and root mean squared errors (RMSE) of the residuals are calculated for forecast horizons of up to 6 days for both PM (Tab. 1) and ΔUT1 (Tab. 2). Note that C04 does contain long-period tidal signals that were removed prior to comparison as recommended in the IERS conventions (*Petit and Luzum*, 2010). As a reference (E0), we also report RMSE calculated from the 305 corresponding Bulletin A forecasts. The accuracy of the terrestrial pole is given in terms of an angle in mas for the two individual components (dx, dy) and the pole offset ($\sqrt{dx^2 + dy^2}$). At the Earth's surface, 1 mas corresponds to a displacement of 3 cm. For comparison, ΔUT1 is expressed in terms of an angle as well (15 mas are equal to 1 ms).

For a first experiment (E1), we apply initial values from Bulletin A at day zero and predict ΔUT1 and PM by integrating ESMGFZ's EAM forecasts forward in time. Consequently, RMSE are identical with E0 for day 0. However, error grow during the subsequent days is slowed down substantially, leading to prediction uncertainties of only 1.76 mas for the pole offset and 2.6 mas for ΔUT1 at day 6, corresponding to an improvement of 41% over the current Bulletin A accuracy. Polar motion prediction in particular benefits from the inclusion of OAM predictions, since atmosphere and ocean dynamics have approximately equal impact on the equatorial components. ΔUT1 is clearly dominated by tropospheric winds, and some information derived from forecasted atmospheric angular momentum is already included in the Bulletin A predictions. The higher temporal resolution of 3 hours and the removal of atmospheric tidal variability from the EAM forecasts issued by ESMGFZ, however, still allows for substantial further improvements.

Prediction critically depends on accurate initial pole coordinates and ΔUT1 estimates that are typically obtained from rapid processing of space geodetic data. In order to quantify the benefit of further improved initial conditions in combination with the final and forecasted EAM functions of ESMGFZ, we perform six experiments that differ from each other only by the assumed latency of the final EOP series. For the second experiment

(E2), we take C04 to be available after 30 days. From that day, PM is integrated forward in time by utilizing the final EAM series provided by ESMGFZ, followed by the 6-day EAM forecasts. Prediction errors at day 0 therefore represent errors introduced by excitations not included in the final EAM series. With 5.23 and 11.9 mas for pole offset and spin rate, respectively, those errors are substantially larger than currently available from Bulletin A. Errors at day 0 decrease with shorter assumed latencies of C04 (experiments E3 – E7), but reach the level of Bulletin A only for a (highly ambitious) latency of 3 days for ΔUT1. For the pole coordinates, even an assumed C04 latency of a single day does not result in better predictions than currently available from Bulletin A.

We also note that in the hypothetical case of perfect initial conditions (i.e., availability of C04 at day zero; experiment H1), prediction accuracies of 1.72 (PM) and 2.2 (ΔUT1) mas can be achieved at day 6. Improvements are also seen for all other forecast horizons as short as 1 day, thereby once more underlining the importance of accurate initial conditions for ΔUT1 and PM prediction. For completeness, we also report results from an even more hypothetical case assuming that in addition to the availability of initial values from C04 also final EAM functions are available for forecasting (H2). In such a setting, accuracies of 1.36 (PM) and 1.7 mas (ΔUT1) are achieved at day 6. Interestingly, only the x-pole is further improved by the final EAM time-series, whereas the y-pole accuracy of 0.9 mas is almost equally well realized by the EAM forecasts. We interpret the results from H2 as the current limit of ΔUT1 and PM forecast accuracy obtainable from contemporary global geophysical fluid models data-sets.

6. Summary

The Earth System Modelling group at Deutsches GeoForschungsZentrum (ESMGFZ) is providing Effective Angular Momentum (EAM) functions that characterize the excitation of the Earth's rotation due to mass re-distribution in atmosphere, oceans, and the terrestrial hydrosphere. The series start in January 1976 with a temporal sampling of up to 3 hours. Periodic signals associated with atmospheric tides and their oceanic response have been estimated and removed prior to the integration of EAM functions. The series are routinely updated every day at around 10 h UTC with all time-steps of the previous day.

In addition to the final EAM functions based on the operational ECMWF analysis data that is constrained by observations, EAM forecasts are also regularly provided for up to 6 days into the future. By means of a hindcast

experiment over the period June 2016 until August 2017, we demonstrated that the incorporation of EAM forecasts reduces the prediction errors down to 1.76 mas for the pole offset and 2.6 mas for ΔUT1 at day 6, corresponding to relative improvements of 41% over Bulletin A. The accuracy at shorter forecast horizons down to 1 day also benefits from the incorporation of forecasted EAM functions, but in particular relies critically on the availability of rapidly processed ΔUT1 and PM estimates from space geodetic observations.

Accurate short-term EOP predictions are a necessity for real-time space applications such as Global Navigation Satellite Systems (GNSS). Many other applications of predicted ΔUT1 and PM values including interplanetary spacecraft tracking, terrestrial astrometry, and operational orbit determination for Earth observation satellites primarily require predictions for a time horizon of about one week, and will therefore directly benefit from improved predictions based on EAM forecasts. This user benefit might be either realized by a routinely generated alternative ΔUT1 and PM prediction product relying on EAM forecasts, or – preferably – by an incorporation of the ESMGFZ's EAM forecasts into the routine processing of Bulletin A as delivered by the IERS.

Acknowledgments

This study has been supported by grant No. DO1311/3-1 of the German Research Foundation (DFG). We thank Deutscher Wetterdienst, Offenbach, Germany, and the European Centre for Medium-Range Weather Forecasts, Reading, U.K., for providing ECMWF operational forecast data. Numerical simulations were performed at Deutsches Klimarechenzentrum, Hamburg, Germany. Both final and forecasted EAM functions are publicly available from www.gfz-potsdam.de/en/esmdata/eam.

Altamimi, Z., P. Rebischung, L. Métivier, and X. Collilieux (2016), ITRF2014: A new release of the International Terrestrial Reference Frame modeling nonlinear station motions, *J. Geophys. Res.*, *121*(8), 6109–6131, doi:10.1002/2016JB013098.

Bizouard, C., and D. Gambis (2009), The combined solution C04 for Earth Orientation Parameters consistent with International Terrestrial Reference Frame 2005, *Int. Assoc. Geod. Symp.*, *134*, 265–270.

Bizouard, C., Zotov, L., and N. Sidorenkov (2014), Lunar influence on equatorial atmospheric angular momentum, *J. Geophys. Res.*, *119(21*, 11,920–11,931.

Brzeziński, A. (1992), Polar motion excitation by variations of the effective angular momentum function: considerations concerning deconvolution problem, *Manuscripta Geodaetica*, *17*(1), 3–20.

Chen, J. (2005), Global mass balance and the length-of-day variation, *J. Geophys. Res.*, *110*(8), 1–10, doi:10.1029/2004JB003474.

Dee, D. P., S. M. Uppala, A. J. Simmons et al. (2011), The ERA-Interim reanalysis: configuration and performance of the data assimilation system, *Q. J. R. Meteorol. Soc.*, *137*(656), 553–597, doi:10.1002/qj.828.

Dill, R. (2008), Hydrological model LSDM for operational Earth rotation and gravity field variations, *Tech. rep.*, Scientific Technical Report 08/09, GFZ, Potsdam, doi:10.2312/GFZ.b103-08095.

Dill, R., and H. Dobslaw (2010), Short-term polar motion forecasts from Earth system modeling data, *Journal of Geodesy*, *84*(9), 529–536.

Dill, R., and H. Dobslaw (2013), Numerical simulations of global-scale high-resolution hydrological crustal deformations, *J. Geophys. Res.*, *118*(9), 5008–5017, doi:10.1002/jgrb.50353.

Dill, R., H. Dobslaw, and M. Thomas (2013), Combination of modeled short-term angular momentum function forecasts from atmosphere, ocean, and hydrology with 90-day EOP predictions, *J. Geodesy*, *87*(6), 567–577, doi:10.1007/s00190-013-0631-6.

Dobslaw, H. (2016), Homogenizing surface pressure time-series from operational numerical weather prediction models for geodetic applications, *J. Geod. Sci.*, *6*, 61–68, doi:10.1515/jogs-2016-0004.

Dobslaw, H., and M. Thomas (2005), Atmospheric induced oceanic tides from ECMWF forecasts, *Geophys. Res. Lett.*, *32*(10), L10,615, doi:10.1029/2005GL022990.

Dobslaw, H., R. Dill, A. Grötzsch, A. Brzeziński, and M. Thomas (2010), Seasonal polar motion excitation from numerical models of atmosphere, ocean, and continental hydrosphere, *J. Geophys. Res.*, *115*, B10,406, doi:10.1029/2009JB007127.

Dobslaw, H., I. Bergmann-Wolf, R. Dill, L. Poropat, M. Thomas, C. Dahle, S. Esselborn, R. Koenig, and F. Flechtner (2017), A new high-resolution model of non-tidal atmosphere and ocean mass variability for de-aliasing of satellite gravity observations: AOD1B RL06, *Geophys. J. Int.*, *211*, 263–269, doi:10.1093/gji/ggx302.

Freedman, A. P., J. A. Steppe, J. O. Dickey, T. M. Eubanks, and L. Y. Sung (1994), The Short-Term Prediction of Universal Time and Length-Of-Day Using Atmospheric Angular Momemtum, *J. Geophys. Res.*, *99*(10), 6981–6996.

Gambis, D., D. A. Salstein, and S. Lambert (2011), Use of atmospheric angular momentum forecasts for UT1 predictions: Analyses over CONT08, *J. Geodesy*, *85*(7), 435–441, doi:10.1007/s00190-011-0479-6.

Gross, R. S. (2007), Earth Rotation Variations - Long Period, *Treatise on Geophysics*, *3*, 239–294, doi:10.1016/B978-044452748-6.00057-2.

Gross, R. S., T. M. Eubanks, J. A. Steppe, A. P. Freedman, J. O. Dickey, and T. F. Runge (1998), A Kalman-filter-based approach to combining independent Earth-orientation series, *J. Geodesy*, *72*(4), 215–235, doi:10.1007/s001900050162.

Gross, R. S., I. Fukumori, and D. Menemenlis (2003), Atmospheric and oceanic excitation of the Earth's wobbles during 1980-2000, *J. Geophys. Res.*, *108*(B8), 2370, doi:10.1029/2002JB002143.

Hagemann, S., and L. Dümenil (2003), Improving a subgrid runoff parameterization scheme for climate models by the use of high-resolution data derived from satellite observations, *Clim. Dyn.*, *21*(3-4), 349–359, doi:10.1007/s00382-003-0349-x.

Jungclaus, J. H., N. Fischer, H. Haak, K. Lohmann, J. Marotzke, D. Matei, U. Mikolajewicz, D. Notz, and J. S. von Storch (2013), Characteristics of the ocean simulations in the Max Planck Institute Ocean Model (MPIOM) the ocean component of the MPI-Earth system model, *Journal of Advances in Modeling Earth Systems*, *5*(2), 422–446, doi:10.1002/jame.20023.

Kalarus, M., H. Schuh, W. Kosek, O. Akyilmaz, C. Bizouard, D. Gambis, R. Gross, B. Jovanović, S. Kumakshev, H. Kutterer, P. J. Mendes

Cerveira, S. Pasynok, and L. Zotov (2010), Achievements of the Earth orientation parameters prediction comparison campaign, *J. Geodesy*, *84*(10), 587–596, doi:10.1007/s00190-010-0387-1.

Madzak, M., M. Schindelegger, J. Boehm, W. Bosch, J. Hagedoorn (2016), High-frequency Earth rotation variations deduced from altimetry-based ocean tides, *J. Geodesy*, *90*(11), 1237?1253, doi:10.1007/s00190-016-0919-4.

Nastula, J., R. M. Ponte, and D. Salstein (2007), Comparison of polar motion excitation series derived from GRACE and from analyses of geophysical fluids, *Geophys. Res. Lett.*, *34*(11), 2–7, doi:10.1029/2006GL028983.

Petit, G., and B. Luzum (2010), *IERS Conventions (2010)*, 1–179 pp., Verlag des Bundesamts für Kartographie und Geodäsie, Frankfurt.

Schindelegger, M., and H. Dobslaw (2016), A global ground truth view of the lunar air pressure tide L 2, *J. Geophys. Res.*, *121*(1), 95–110, doi:10.1002/2015JD024243.

Schindelegger, M., D. Einšpigel, D. Salstein, and J. Böhm (2016), The Global S1 Tide in Earth's Nutation, *Surv. Geophys.*, *37*(3), 643–680, doi:10.1007/s10712-016-9365-3.

Uppala, S. M., P. Kallberg, A. J. Simmons et al. (2005), The ERA-40 reanalysis, *Q. J. R. Meteorol. Soc.*, *131*, 2961–3012, doi:10.1256/qj.04.176.

von Storch, H., and F. W. Zwiers (1999), *Statistical analysis in climate research*, 485 pp., Cambridge Univ. Press, Cambridge, U.K., doi:10064289.

Yan, H., and B. F. Chao (2012), Effect of global mass conservation among geophysical fluids on the seasonal length of day variation, *J. Geophys. Res.*, *117*(2), 95–110, doi:10.1029/2011JB008788.

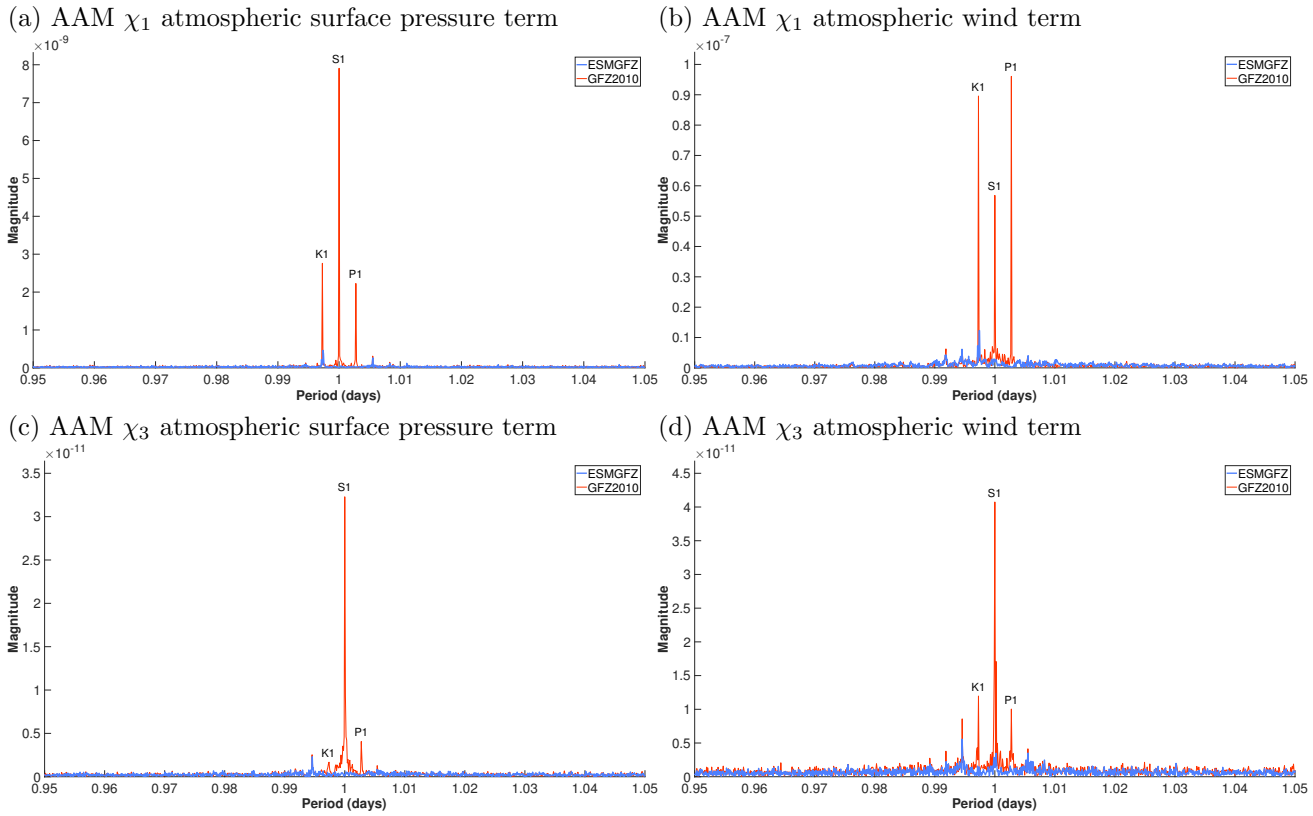

Figure 1: Diurnal tidal signals contained in atmospheric EAM functions of ESMGFZ (blue) and the outdated version GFZ2010 (grey): (a) χ_1 atmospheric surface pressure term, (b) χ_1 atmospheric wind term, (c) χ_3 atmospheric surface pressure term, and (d) χ_3 atmospheric wind term.

Table 1: Root mean squared errors of nine different hindcast experiments extending from June 2016 until August 2017 for the prediction of x and y pole coordinates [mas] as evaluated against C04 for forecast horizons of up to 6 days: Bulletin A as routinely issued by IERS (E0); EAM forecasts from ESMGFZ and initial values from Bulletin A at day 0 (E1); EAM forecasts from ESMGFZ and initial values from C04 at different lags from -30 to -1 days (E2 – E7). We further present results of two hypothetical experiments with perfect initial conditions (H1); and in addition also perfect EAM forecasts taken from the final EAM functions (H2) as indicators for the current polar motion forecast accuracy limit.

ID	Predictor	Initial Value	day 0	day 1	day 2	day 3	day 4	day 5	day 6
						x-pole [mas]			
E0	Bulletin A	Bulletin A: day 0	0.07	0.35	0.76	1.23	1.69	2.11	2.49
E1	EAM forecasts	Bulletin A: day 0	0.07	0.31	0.59	0.85	1.05	1.26	1.47
E2	EAM forecasts	EOP C04: day -30	4.07	4.22	4.49	4.75	4.95	5.13	5.33
E3	EAM forecasts	EOP C04: day -10	1.43	1.56	1.79	2.02	2.21	2.38	2.58
E4	EAM forecasts	EOP C04: day -6	1.03	1.17	1.40	1.64	1.83	2.01	2.20
E5	EAM forecasts	EOP C04: day -4	0.74	0.90	1.14	1.37	1.57	1.76	1.96
E6	EAM forecasts	EOP C04: day -2	0.46	0.61	0.83	1.10	1.30	1.48	1.69
E7	EAM forecasts	EOP C04: day -1	0.27	0.46	0.70	0.95	1.16	1.35	1.55
H1	EAM forecasts	EOP C04: day 0	0.00	0.28	0.56	0.82	1.02	1.22	1.43
H2	final EAM	EOP C04: day 0	0.00	0.27	0.46	0.60	0.73	0.88	1.02
						y-pole [mas]			
E0	Bulletin A	Bulletin A: day 0	0.05	0.24	0.49	0.78	1.08	1.36	1.62
E1	EAM forecasts	Bulletin A: day 0	0.05	0.24	0.40	0.55	0.69	0.83	0.96
E2	EAM forecasts	EOP C04: day -30	3.29	3.41	3.53	3.65	3.79	3.91	4.01
E3	EAM forecasts	EOP C04: day -10	1.29	1.41	1.51	1.61	1.72	1.82	1.91
E4	EAM forecasts	EOP C04: day -6	0.95	1.07	1.18	1.30	1.42	1.53	1.63
E5	EAM forecasts	EOP C04: day -4	0.67	0.81	0.92	1.05	1.17	1.29	1.41
E6	EAM forecasts	EOP C04: day -2	0.39	0.54	0.66	0.80	0.93	1.06	1.18
E7	EAM forecasts	EOP C04: day -1	0.23	0.39	0.52	0.66	0.80	0.93	1.05
H1	EAM forecasts	EOP C04: day 0	0.00	0.23	0.39	0.55	0.68	0.82	0.95
H2	final EAM	EOP C04: day 0	0.00	0.23	0.39	0.53	0.66	0.78	0.90

Table 2: Root mean squared errors of nine different hindcast experiments extending from June 2016 until August 2017 for the prediction of ΔUT1 [mas; with 15 mas = 1ms] as evaluated against C04 for forecast horizons of up to 6 days: Bulletin A as routinely issued by IERS (E0); EAM forecasts from ESMGFZ and initial values from Bulletin A at day 0 (E1); EAM forecasts from ESMGFZ and initial values from EOP C04 at different lags from -30 to -1 days (E2 – E7). We further present results of two hypothetical experiments with perfect initial conditions (H1); and in addition also perfect EAM forecasts taken from the final EAM functions (H2) as indicators for the current ΔUT1 forecast accuracy limit.

ID	Predictor	Initial Value	day 0	day 1	day 2	day 3	day 4	day 5	day 6
			ΔUT1 [mas]						
E0	Bulletin A	Bulletin A: day 0	1.2	1.8	2.1	2.4	2.9	3.5	4.4
E1	EAM forecasts	Bulletin A: day 0	1.2	1.2	1.4	1.7	1.8	2.1	2.6
E2	EAM forecasts	EOP C04: day -30	11.9	12.5	13.2	13.7	14.3	14.9	15.3
E3	EAM forecasts	EOP C04: day -10	2.6	2.9	3.0	3.3	3.8	4.1	4.4
E4	EAM forecasts	EOP C04: day -6	1.7	2.0	2.1	2.4	2.7	3.0	3.5
E5	EAM forecasts	EOP C04: day -4	1.4	1.5	1.8	2.0	2.3	2.6	3.0
E6	EAM forecasts	EOP C04: day -2	0.9	1.2	1.4	1.5	1.8	2.1	2.6
E7	EAM forecasts	EOP C04: day -1	0.6	0.8	1.1	1.4	1.5	2.0	2.4
H1	EAM forecasts	EOP C04: day 0	0.0	0.6	0.9	1.2	1.4	1.8	2.2
H2	final EAM	EOP C04: day 0	0.0	0.6	0.6	1.1	1.4	1.5	1.7

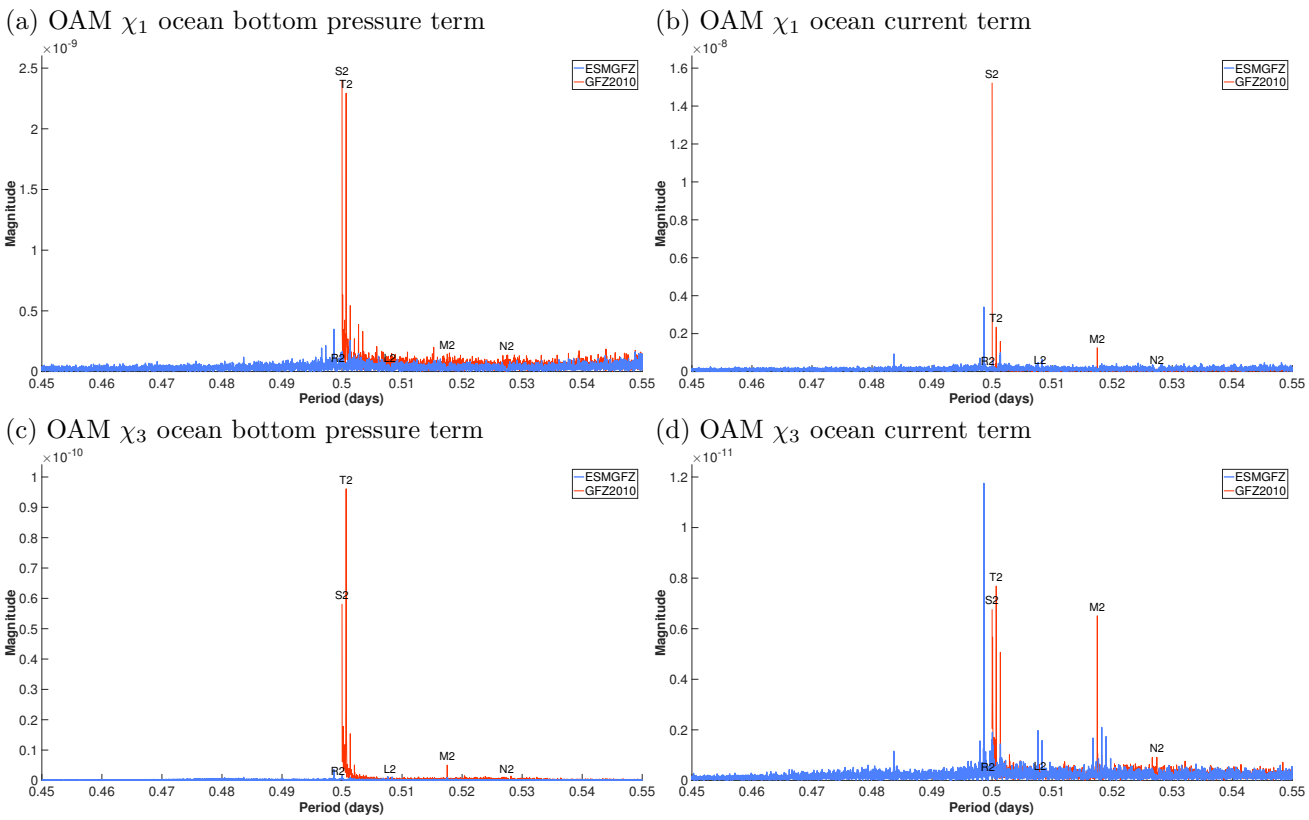

Figure 2: Semi-diurnal tidal signals contained in oceanic EAM functions of ESMGFZ (blue) and the outdated version GFZ2010 (grey): (a) χ_1 ocean bottom pressure term, (b) χ_1 ocean current term, (c) χ_3 ocean bottom pressure term, and (d) χ_3 ocean current term.

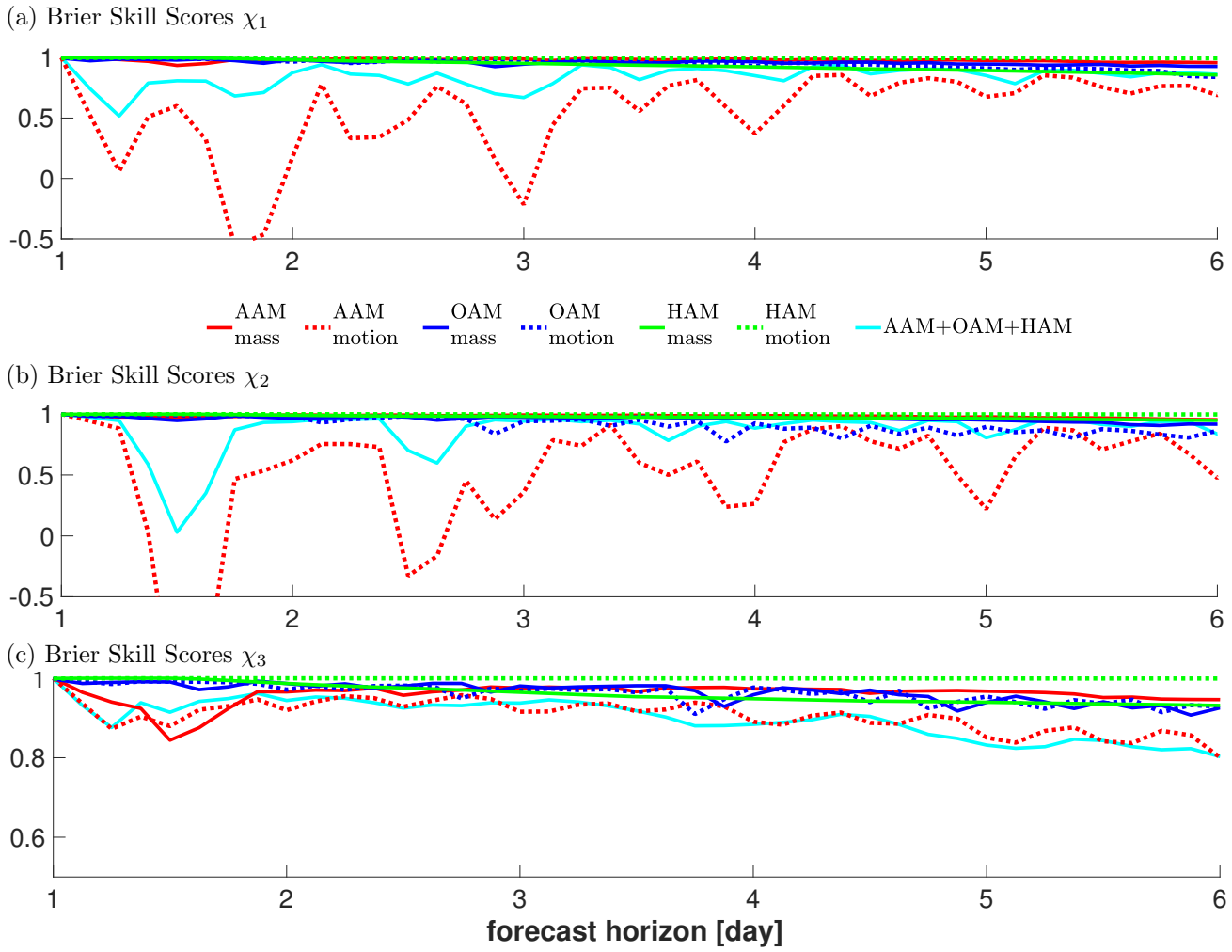

Figure 3: Brier skill scores obtained from a hindcast experiment extending from January 2016 until June 2017 of 6 days-long EAM forecasts verified against final EAM functions from ESMGFZ for individual matter and motion terms of AAM, OAM and HAM as well as their sum for (a) χ_1, (b) χ_2, and (c) χ_3.

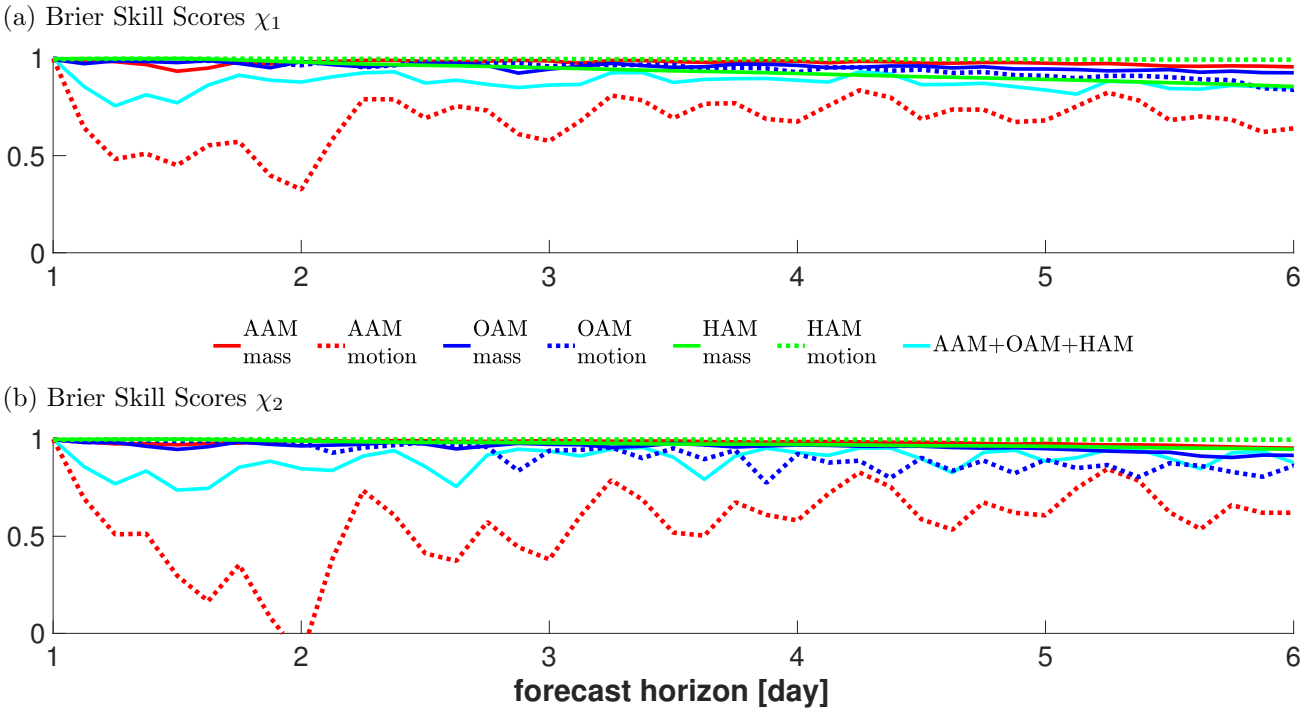

Figure 4: Same as Fig. 3, but AAM motion terms are additionally filtered with a 24 h lowpass filter before calculating Brier skill scores for (a) χ_1, and (b) χ_2.